

Article

In Search of Preferential Macrocyclic Hosts for Sulfur Mustard Sensing and Recognition: A Computational Investigation through the New Composite Method r²SCAN-3c of the Key Factors Influencing the Host-Guest Interactions

Fatine Ali Messiad ^{1,2}, Nesrine Ammouchi ^{2,3,*}, Youghourta Belhocine ^{1,*} , Hanan Alhussain ⁴ ,
Monira Galal Ghoniem ⁴, Ridha Ben Said ^{5,6}, Fatima Adam Mohamed Ali ⁴ and Seyfeddine Rahali ^{5,*} 

- ¹ Department of Process Engineering, Faculty of Technology, Université 20 Août 1955, El Hadaik Road, Skikda 21000, Algeria; f.alimessiad@univ-skikda.dz
- ² LRPCSI-Laboratoire de Recherche sur la Physico-Chimie des Surfaces et Interfaces, Université 20 Août 1955, Skikda 21000, Algeria
- ³ Département de Technologie, Faculté de Technologie, Université 20 Août 1955, B.P. 26, Route d'El Hadaiek, Skikda 21000, Algeria
- ⁴ Department of Chemistry, College of Science, Imam Mohammad Ibn Saud Islamic University (IMSIU), Riyadh 11432, Saudi Arabia; hmalhussain@imamu.edu.sa (H.A.); mgghoniem@imamu.edu.sa (M.G.G.); famohamedali@imamu.edu.sa (F.A.M.A.)
- ⁵ Department of Chemistry, College of Science and Arts, Qassim University, P.O. 53, Ar Rass 51921, Saudi Arabia; ben.said.ridha@gmail.com
- ⁶ Laboratoire de Caractérisations, Applications et Modélisations des Matériaux, Faculté des Sciences de Tunis, Université Tunis El Manar, Tunis 2092, Tunisia
- * Correspondence: n.ammouchi@univ-skikda.dz (N.A.); y.belhocine@univ-skikda.dz (Y.B.); saif.rahali@gmail.com (S.R.)



Citation: Messiad, F.A.; Ammouchi, N.; Belhocine, Y.; Alhussain, H.; Ghoniem, M.G.; Said, R.B.; Ali, F.A.M.; Rahali, S. In Search of Preferential Macrocyclic Hosts for Sulfur Mustard Sensing and Recognition: A Computational Investigation through the New Composite Method r²SCAN-3c of the Key Factors Influencing the Host-Guest Interactions. *Nanomaterials* **2022**, *12*, 2517. <https://doi.org/10.3390/nano12152517>

Academic Editor:
Diego Cazorla-Amorós

Received: 29 June 2022
Accepted: 19 July 2022
Published: 22 July 2022

Publisher's Note: MDPI stays neutral with regard to jurisdictional claims in published maps and institutional affiliations.

Abstract: Sulfur mustard (SM) is a harmful warfare agent that poses a serious threat to human health and the environment. Thus, the design of porous materials capable of sensing and/or capturing SM is of utmost importance. In this paper, the interactions of SM and its derivatives with ethylpillar[5]arene (EtP[5]) and the interactions between SM and a variety of host macrocycles were investigated through molecular docking calculations and non-covalent interaction (NCI) analysis. The electronic quantum parameters were computed to assess the chemical sensing properties of the studied hosts toward SM. It was found that dispersion interactions contributed significantly to the overall complexation energy, leading to the stabilization of the investigated systems. DFT energy computations showed that SM was more efficiently complexed with DCMP[5] than the other hosts studied here. Furthermore, the studied macrocyclic containers could be used as host-based chemical sensors or receptors for SM. These findings could motivate experimenters to design efficient sensing and capturing materials for the detection of SM and its derivatives.

Keywords: non-covalent interactions; sulfur mustard; macrocycles; DFT-D4; inclusion complex; sensing



Copyright: © 2022 by the authors. Licensee MDPI, Basel, Switzerland. This article is an open access article distributed under the terms and conditions of the Creative Commons Attribution (CC BY) license (<https://creativecommons.org/licenses/by/4.0/>).

1. Introduction

Ethylene dichloride sulfide (bis(2-chloroethyl) sulfide) commonly known as sulfur mustard (SM) is a cytotoxic chemical compound with an oily liquid appearance belonging to the category of mass destruction weapons [1–3]. SM was first prepared in 1822 by César Despretz, however, it was not used until 1917 during the First World War [4]. SM is a highly toxic agent that attacks clammy skin, tissues, and airways, causing severe blisters and chemical burns to the eyes and mucous membranes, as well as long-term genetic damage [5,6]. In addition to its effects on health, SM is dangerous for the environment and

can cause harmful effects on aquatic organisms. In this regard, addressing the problem of this chemical warfare agent and its derivatives is of particular importance.

Some decontamination processes have been developed to eliminate the SM such as chemical degradation by hydrolysis or oxidation [7,8]. An alternative strategy, based on the complexation of harmful substances [9–12] by macrocyclic systems offers new perspectives to address the issue of capturing and storing hazardous substances. Supramolecular chemistry is mainly concerned with the study of the host-guest complexes in which two or more neutral or charged molecules bind to each other via non-covalent interactions [13–15]; these interactions are the main driving forces of the complexation process, which leads to the modification of the physicochemical properties of host-guest complexes [16–20]. Among the supramolecular systems, cyclodextrins [21,22], cucurbiturils [23–25], calixarenes [26–29], and pillararenes [30–32] are the most studied host compounds. Moreover, self-assembled supramolecular architectures and nanostructures [33–38] play a key role in nanotechnologies and bioengineering.

In this context, Li et al. [39] conducted an experimental study in which per-ethylated pillar[5]arene (EtP[5]) host was used as a macrocyclic receptor for the recognition of the SM and its derivatives. The authors observed a strong binding and capture abilities toward SM and its stimulants with proven stability for a period of time (at least six months in the crystals) and discussed the mechanism of the interactions between (EtP[5]) and the guests SM, 2-chloroethyl ethyl sulfide (S1), bis(2-chloroethyl) ether (S2), 2-chloroethyl ethyl ether (S3), 1,5-dichloropentane (S4), and 1-chloropentane (S5). The optimized structures of SM and its stimulants (S1–S5) are represented in Figure 1.

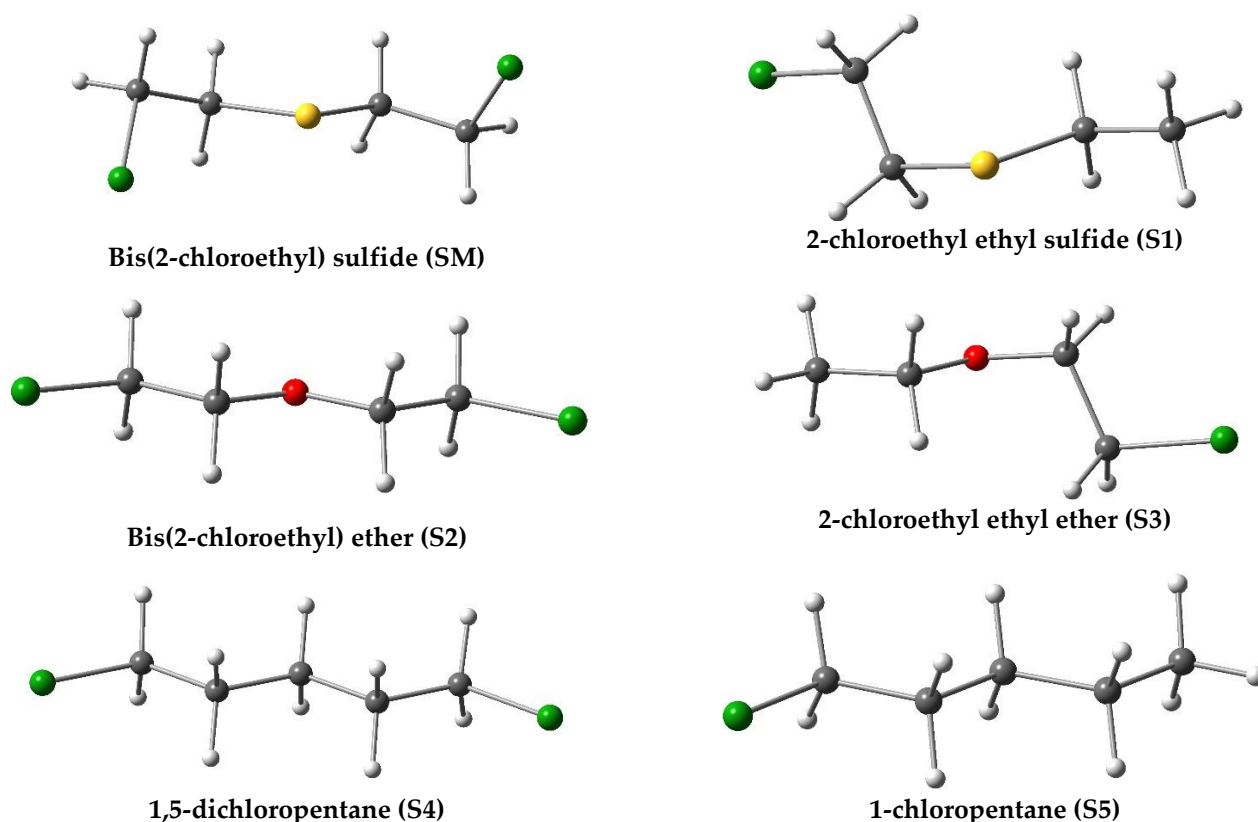


Figure 1. Optimized molecular structures of the guests: SM, S1, S2, S3, S4, and S5. Atom colors: chlorine (green); oxygen (red); carbon (grey); sulfur (yellow) and hydrogen (white).

From Figure 1, it is clear that S2 and S4 have a similar structure to that of SM, with the central sulfur atom replaced by oxygen or carbon atoms, respectively. The guests S3 and S5 are the monofunctional analogs of S2 and S4. X-ray diffraction showed that EtP[5] forms 1:1 inclusion complex with all the guests (SM–S5). The inclusion process is mainly driven by

multiple C–H... π /Cl/S/O interactions. As a limitation of the study, the crystalline EtP[5] cannot be used for the degradation of SM. Therefore, it is interesting to functionalize the macrocyclic host systems as a strategy for the detoxification of SM [40], which may result in increasing the interaction energy and time storage.

Computational chemistry plays a crucial role in the field of host–guest complexation chemistry as an efficient tool for investigating the mechanism of the inclusion process [41–44] and for the prediction of new host molecules that can efficiently encapsulate the drug guests [45,46]. In this work, we present a DFT-D4 study of the host-guest interactions between the per-ethylated pillar[5]arene and SM and its simulants. Another important point of interest was to investigate the possible complexation of SM with several macrocyclic systems including functionalized pillar[5]arenes. Furthermore, different computational tools were used to analyze the structural, electronic, and sensing properties as well as the intermolecular interactions responsible for the stability of the formed complexes. We believe that this work will be useful for future experimental investigations aiming at capturing or sensing SM and its derivatives or analogs [47,48] using functionalized macrocyclic hosts.

2. Computational Methods

Full geometry optimization and energy calculations were performed using the recently developed meta-generalized-gradient approximation (mGGA) composite method r²SCAN-3c [49–57] combined with a modified version of the def2-TZVP basis set [58] denoted def2-mTZVPP [49]. A geometrical counterpoise correction (gCP) for the intra- and inter-molecular basis set superposition error was employed [59], as well as the Grimme dispersion term based on tight-binding partial charges (D4) [60–62] that was applied to account for the dispersion correction. All the DFT calculations were carried out with the ORCA program package (version 5.0.0) [63–65] in the gas phase. The complexation process between SM and its simulants and EtP[5] was also evaluated in *o*-xylene using the conductor-like polarizable continuum model (CPCM) [66,67]. The complexation energy ($E_{\text{complexation}}$) for the SM and its derivatives with the studied macrocyclic hosts is computed by the following equation:

$$E_{\text{complexation}} = E_{\text{(complex)}} - (E_{\text{(host)}} + E_{\text{(guest)}}) \quad (1)$$

where $E_{\text{(host)}}$ is the energy of the host molecule, $E_{\text{(complex)}}$ is the energy of the host-guest complex, and $E_{\text{(guest)}}$ is the energy of the guest molecule.

3. Results and Discussion

3.1. Interaction of SM and Its Simulants with EtP[5]

The starting geometries for the DFT geometry optimization of SM@EtP[5], S1@EtP[5], S2@EtP[5], S3@EtP[5], S4@EtP[5], and S5@EtP[5] complexes were retrieved from the crystal X-ray structures [39], corresponding, respectively, to the following assigned CCDC numbers 1831237 [68], 1884850 [69], 1831239 [70], 1884851 [71], 1831240 [72], and 1884852 [73].

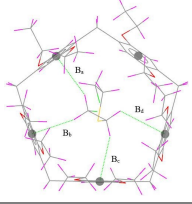
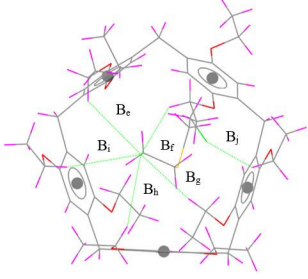
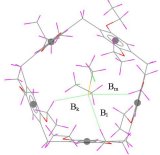
3.1.1. Structural and Energetic Properties

The optimized geometry and the values of the nearest intermolecular distances between SM and EtP[5] in SM@EtP[5] are visualized with Mercury 4.0 program [74] and presented in Table 1. The host-guest process is consisting of 1:1 ratio, in which non-covalent interactions play an important role in the stabilization of the formed complexes.

From a comparison of the experimental and optimized SM@EtP[5] complex geometries shown in Table 1, it is quite clear that the experimentally observed C–H... π /S/Cl intermolecular distances are reasonably reproduced in the gas phase by the r²SCAN-3c composite method. The sum of the deviations from the C–H... π experimental intermolecular distances noted ΔB in Table 1, obtained with r²SCAN-3c is 0.58 Å. The C–H...Cl

and particularly the C–H...S hydrogen bond lengths are better predicted by r^2 SCAN-3c ($\Delta B_{C-H...Cl} = 0.36 \text{ \AA}$, $\Delta B_{C-H...S} = 0.21 \text{ \AA}$).

Table 1. Experimental and computed nearest intermolecular distances (\AA) of SM@EtP[5] complex. (The values in brackets represent the difference between the computed and the experimental distances).

Interaction	Interaction Distance	r^2 SCAN-3c	Exp. [39]	Gas-Phase Optimized Geometries
C–H... π	B _a	2.82 (0.01)	2.81	
	B _b	2.55 (0.13)	2.68	
	B _c	2.56 (0.18)	2.74	
	B _d	2.70 (0.26)	2.96	
	ΔB	0.58	-	
C–H...Cl	B _e	3.02 (0.20)	3.22	
	B _f	3.05 (0.03)	3.08	
	B _g	3.35 (0.01)	3.34	
	B _h	3.14 (0.06)	3.20	
	B _i	3.19 (0.04)	3.15	
	B _j	3.34 (0.02)	(3.32)	
	ΔB	0.36	-	
C–H...S	B _k	3.24 (0.08)	3.32	
	B _l	3.01 (0.11)	3.12	
	B _m	3.18 (0.02)	3.16	
	ΔB	0.21	-	

In addition to the geometric parameters, the complexation energies were calculated with r^2 SCAN-3c in gas and *o*-xylene media (Table 2). The gas-phase dispersion-corrected energies were also evaluated and listed in Table 2.

Table 2. Calculated complexation and dispersion-corrected energies (kJ/mol) and experimental values of association constants in M^{-1} .

Complex	r^2 SCAN-3c (Gas Phase)	r^2 SCAN-3c (O-Xylene)	r^2 SCAN-3c Gas Phase Dispersion Energy	Association Constants (M^{-1}) [39]
SM@EtP[5]	−141	−114.44	−55.48	6.2×10^3
S1@EtP[5]	−122.74	−105.69	−51.03	2.9×10^2
S2@EtP[5]	−133.76	−113.01	−50.31	1.3×10^3
S3@EtP[5]	−110.36	−97.43	−46.66	67
S4@EtP[5]	−144.92	−118.35	−53.72	1.8×10^4
S5@EtP[5]	−119.69	−103.09	−50.09	7.9×10^2

Based on the association constant values of the six complexes determined by Li et al. [39], the ranking in the decreasing order follows the sequence $K_a(S4) > K_a(SM) > K_a(S2) > K_a(S5) > K_a(S1) > K_a(S3)$. The same trend was observed (both in the gas phase and in *o*-xylene) by the calculated complexation energies with r^2 SCAN-3c except for S1@EtP[5] and S5@EtP[5]. Gas-phase complexation energies are −144.92, −141, −133.8, −122.74, −119.69, and −110.36 kJ/mol for S4@EtP[5], SM@EtP[5], S2@EtP[5], S1@EtP[5], S5@EtP[5], and S3@EtP[5], respectively. The computed complexation energies in *o*-xylene are found to

be less negative. The results show that r^2 SCAN-3c calculations are in good agreement with the experimental association constants. From a structural and energetic point of view, the r^2 SCAN-3c describes well the systems studied in this work and will be therefore employed for subsequent calculations. The calculated dispersion energies with r^2 SCAN-3c functional in gas phase for SM@EtP[5], S1@EtP[5], S2@EtP[5], S3@EtP[5], S4@EtP[5], and S5@EtP[5] are, respectively, -55.48 , -51.03 , -50.31 , -46.66 , -53.72 , and -50.09 kJ/mol (Table 2). The most stable complexes SM@EtP[5] and S4@EtP[5] have the highest dispersion energies of -55.48 and -53.72 kJ/mol whereas the less stable complex S3@EtP[5] has the lowest dispersion energy (-46.66 kJ/mol), indicating that dispersion interactions contribute significantly to the formation and stabilization of the complexes.

3.1.2. Electronic Properties of SM, S1, S2, S3, S4, and S5@EtP[5] Complexes

For EtP[5] and all formed complexes, the chemical parameters such as frontier molecular orbitals (HOMO and LUMO), HOMO-LUMO energy gap [75,76], the percentage of HOMO-LUMO gap variation $|\Delta E_g| \%$ [77] and the dipole moment (μ) [78] were calculated in gas phase using r^2 SCAN-3c functional. The results are reported in Table 3.

Table 3. Calculated chemical parameters for EtP[5] and all complexes using r^2 SCAN-3c in the gas phase.

Complex	HOMO (eV)	LUMO (eV)	H-L gap (eV)	$ \Delta E_g \%$	μ (Debye)
EtP[5]	-4.38	-0.87	3.51	-	0.06
SM@EtP[5]	-4.44	-1.06	3.38	3.85	3.44
S1@EtP[5]	-4.43	-0.95	3.48	0.84	1.87
S2@EtP[5]	-4.47	-1.01	3.46	1.42	0.88
S3@EtP[5]	-4.41	-0.97	3.44	1.99	1.87
S4@EtP[5]	-4.44	-1.07	3.37	3.99	2.11
S5@EtP[5]	-4.43	-0.98	3.45	1.71	1.82

As shown in Table 3, the HOMO, LUMO and HOMO-LUMO (H-L) gap energies are slightly varied upon the complexation of SM and its stimulants with EtP[5], however, the percentage of variation of HOMO-LUMO gap and the electric dipole moment of the two most stable complexes (SM@EtP[5] and S4@EtP[5]) are the highest among all complexes. The variation of |H-L| energy gap of SM@EtP[5] and S4@EtP[5] decreased, respectively, by 3.85 and 3.99 % after the complexation of SM and S4.

3.1.3. NCI-RDG and IGMH Analysis of the Host-Guest Interactions

The identification of intra- and intermolecular interactions in supramolecular chemistry is important for quantifying the non-covalent forces responsible for the host-guest recognition [79].

Non-covalent interaction (NCI) analysis of reduced density gradient (RDG) [80] and independent gradient model based on Hirshfeld partition (IGMH) [81] can provide insights into the nature of host-guest interactions through the drawing of 3D color-filled isosurfaces representative of the occurring interactions, where blue, green, and red indicate, respectively, strong attractive interactions, van der Waals interactions and steric clashes.

The NCI-RDG isosurfaces (left figures of Figure 2) of all complexes and their scatter plots (right figures of Figure 2) were plotted with an isovalue of 0.5 a.u. in Figure 2. The NCI-RDG and IGM isosurfaces were visualized by VMD 1.9.3 program [82] through the outputs of Multiwfn 3.8 [83].

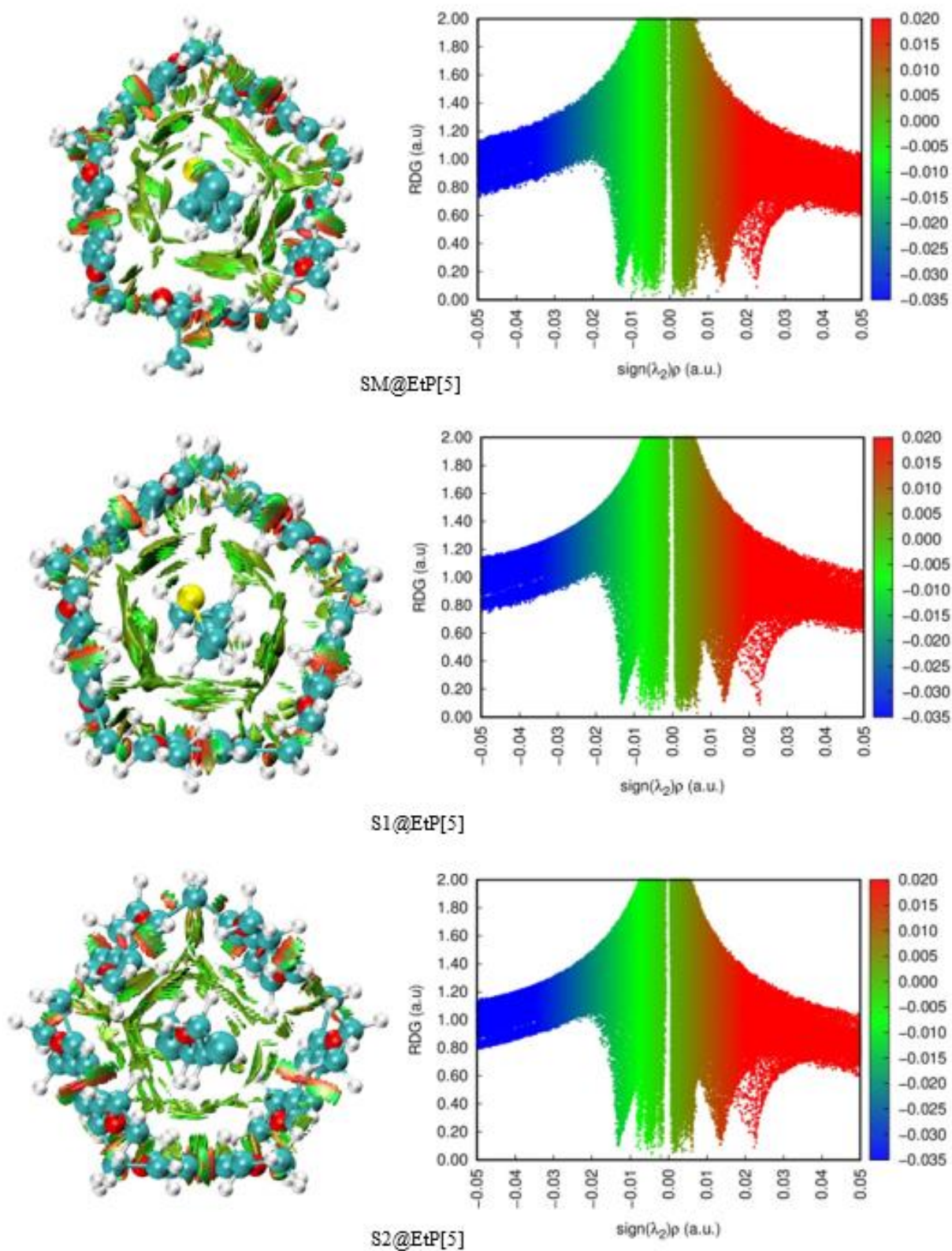


Figure 2. Cont.

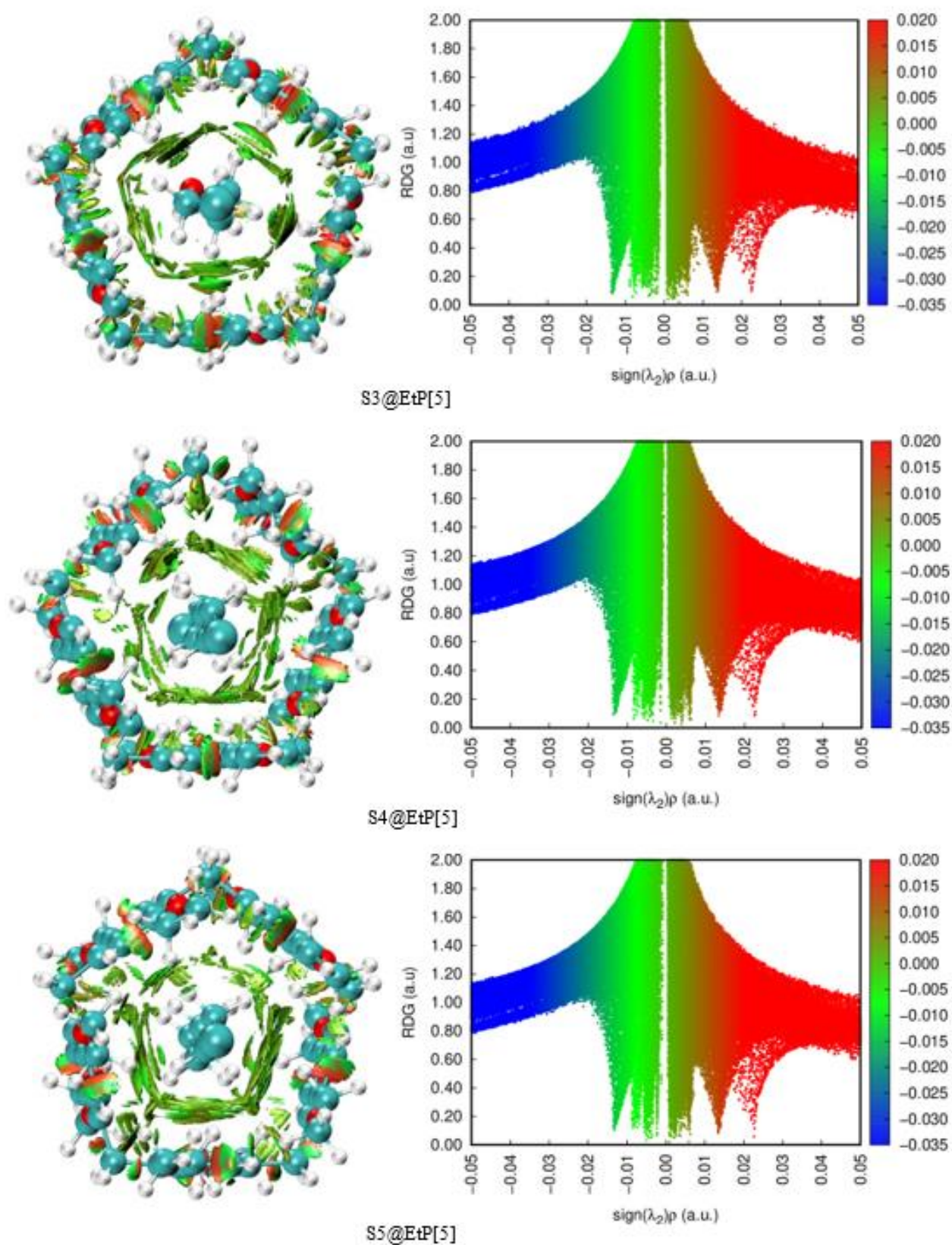


Figure 2. NCI-RDG isosurfaces (isovalue 0.5 a.u.) (left) and scatter plots (right) of SM@EtP[5], S1@EtP[5], S2@EtP[5], S3@EtP[5], S4@EtP[5], and S5@EtP[5].

The visual characterization of NCI-RDG isosurfaces shows the presence of green-colored and light brown regions (left figures of Figure 2) in the interval $[-0.015, 0.01$ a.u.]

indicating that weak dispersive forces are dominant in stabilizing the complex formation between SM and its stimulants, and the EtP[5] host. For SM@EtP[5], the peak occurring near -0.015 a.u. indicates mainly C-H \cdots H-C and C-H \cdots O intramolecular interactions, whereas the peaks in the range of -0.01 to 0.00 a.u. consist of mostly C-H \cdots H-C, S $\cdots\pi$, C-H \cdots Cl, C-H \cdots S, C-H \cdots O and C-H $\cdots\pi$ intermolecular interactions. Similar conclusions are drawn using IGMH analysis (Supplementary data Figure S1).

DFT calculations show that the methylene groups are involved in the intermolecular interactions, indeed, the complex S4@EtP[5] with the highest number of methylene groups (Five CH₂ groups) showed the highest complexation energy, followed by SM@EtP[5], S2@EtP[5], and S5@EtP[5] each with four CH₂ groups and S1@EtP[5], and S3@EtP[5] complexes each with three CH₂ groups. These findings suggest a strong correlation between C-H $\cdots\pi$ intermolecular interactions and the stability of the formed complexes [84]. The lower complexation energies of S2@EtP[5] and S3@EtP[5] in comparison, respectively, with SM@EtP[5], S4@EtP[5], and S1@EtP[5], S5@EtP[5] are due to the absence of intermolecular interactions between the central oxygen atom of S2 and S3 and the benzene moieties of EtP[5].

Due to their additive effect, the weak attractive C-H $\cdots\pi$ interactions play a key role as an important driving force in the inclusion process of SM and its derivatives within EtP[5].

DFT results indicated that weak hydrogen and halogen bonding (C-H \cdots S, C-H \cdots O and C-H \cdots Cl) was overall observed in the studied complexes.

3.2. Interactions between SM and Different Macrocyclic Hosts

The interaction of SM with eight macrocyclic hosts namely, pillar[5]arene (P[5]) [85], methylpillar[5]arene (MeP[5]) [32], Deca(carboxymethoxy)pillar[5]arene (DCMP[5]) [86–88], Pillar[5]quinone (P[5]Q) [89], mono(2,5-diamino-1,4-benzoquinone)pillar[5]arene (DAP[5]) [90], cucurbit[6]uril (CB[6]) [91], calix[5]arene (CX[5]) [92,93] and β -cyclodextrin (β -CD) [94,95] was studied computationally in gas phase using the r^2 SCAN-3c composite method. The most stable inclusion complexes were calculated based on the method elaborated by Liu and Guo [96]. The center of the guest and the host was set as the center of the coordination system, then SM was translated along the Z-axis from -10 to $+10$ Å with 2 Å step as shown in Figure 3. The complexation energies computed with r^2 SCAN-3c in gas phase as a function of the Z coordinate are displayed in Table 4. The optimized structures exhibit negative complexation energies, indicating an energetic favored process.

The most stable configurations for SM@P[5], SM@MeP[5], SM@DCMP[5], SM@P[5]Q, SM@DAP[5], SM@CB[6], SM@CX[5], and SM@ β -CD with respective energies of -126.79 , -113.16 , -155.26 , -90.77 , -116.51 , -96.94 , -71.42 and -89.07 kJ/mol are located, respectively, at $Z = -2$ Å, $Z = 0$ Å, $Z = 0$ Å, $Z = +8$ Å, $Z = -2$ Å, $Z = +4$ Å, $Z = +8$ Å, and $Z = +2$ Å (Table 4). The geometries of the eight most stable complexes are visualized in Figure 3 using GaussView 5 software [97].

Among the studied hosts, the most important complexation energy was observed for DCMP[5] (-155.3 kJ/mol), which displays the highest complexation energy.

The SM guest is fully entrapped in the DCMP[5] cavity. The analysis of the nearest intermolecular distances occurring in the optimized structure of SM@DCMP[5] shows that there are four C-H $\cdots\pi$ interactions between the methylene groups of SM and the benzene moieties of DCMP[5], with distances ranging from 2.89 to 3.06 Å (Figure 4). Each chlorine atom of SM forms two C-H \cdots Cl hydrogen bonds with the methylene moieties attached to the terminal -COOH groups of DCMP[5] at distances of 2.90 and 3.15 Å. Eleven C-H \cdots O hydrogen bonds ranging from 2.67 to 3.20 Å were also observed between the $-(\text{CH}_2)-$ moieties of SM and the oxygen atoms of the -COOH groups of the host. However, no short C-H \cdots S contacts were found between SM and DCMP[5].

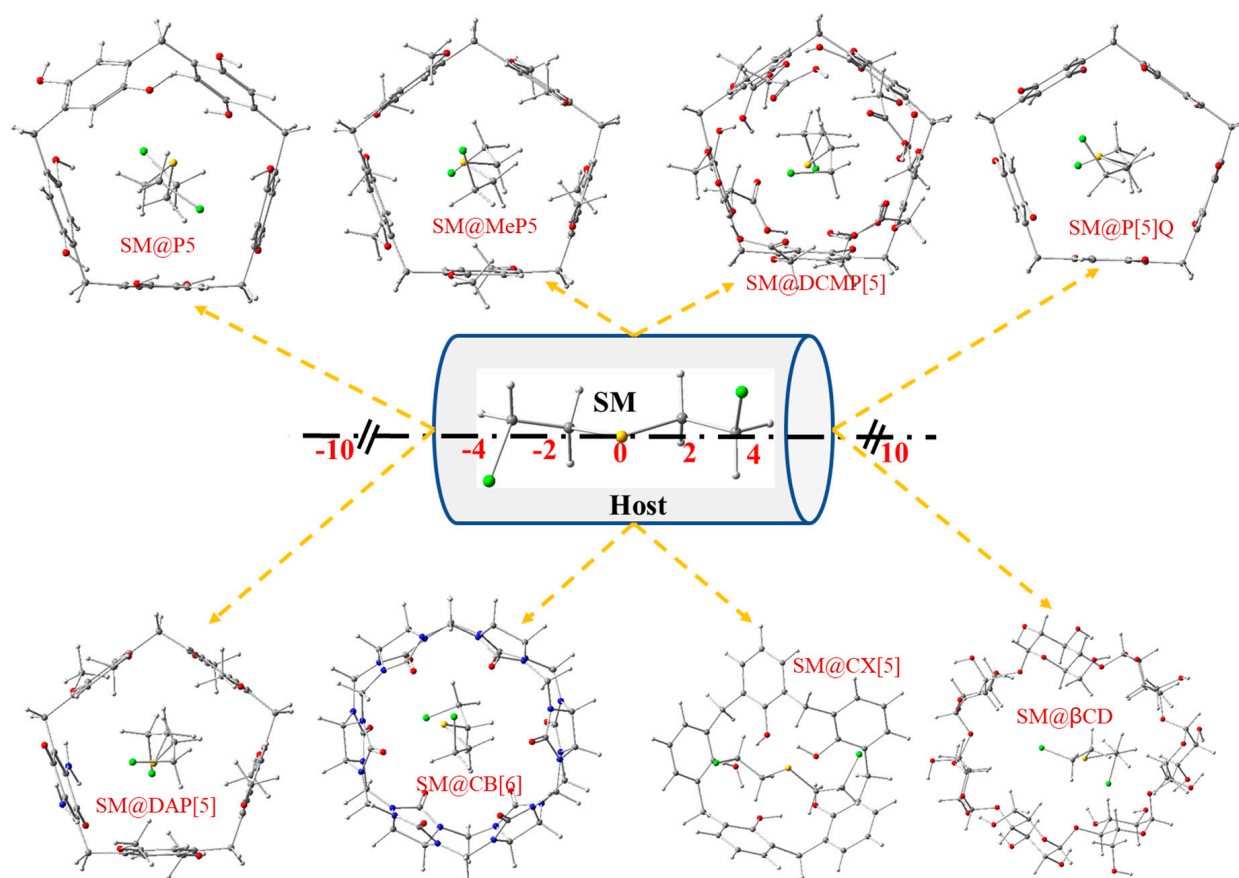


Figure 3. Coordinate systems of the complexation process of SM and eight macrocyclic molecules and the molecular structures of the most stable host-guest complexes. Atom colors: chlorine (green); oxygen (red); carbon (grey); sulfur (yellow); nitrogen (blue) and hydrogen (white).

Table 4. Complexation energies (kJ/mol) between SM and the eight studied macrocycles calculated with r^2 SCAN-3c in the gas phase.

Position (Å)	SM@P[5]	SM@MeP[5]	SM@DCMP[5]	SM@P[5]Q	SM@DAP[5]	SM@CB[6]	SM@CX[5]	SM@β-CD
−10	−54.25	−29.41	−83.32	−90.51	−44.74	−72.12	−32.35	−56.82
−8	−77.19	−109.80	−121.57	−74.96	−71.12	−68.88	−32.77	−52.10
−6	−77.28	−110.00	−121.66	−90.53	−114.52	−75.41	−51.72	−51.61
−4	−123.65	−109.99	−118.70	−87.29	−112.35	−96.42	-	−54.82
−2	−126.79	−110.00	−120.90	−85.67	−116.51	−96.44	-	−55.36
0	−123.62	−113.16	−155.26	−86.63	−112.37	−96.80	-	−79.49
+2	−101.89	−109.90	−128.54	−90.23	−114.22	−95.76	-	−89.07
+4	−101.97	−109.92	−118.63	−90.38	−114.18	−96.94	-	−87.11
+6	−101.67	−109.93	−122.04	−90.33	−114.32	−75.28	−71.41	−85.58
+8	−99.42	−109.66	−80.91	−90.77	−37.20	−69.12	−71.42	−81.01
+10	−99.40	−29.50	−85.44	−90.69	−96.49	−73.44	−53.95	−78.78

3.2.1. Electronic and Chemical Sensing Properties

Due to their efficiency and cost-effectiveness, macrocyclic host systems with cavities are relevant materials for sensing applications in medicine, biology, and environmental monitoring. The performance of such materials can be improved by introducing in their structures specific functional groups that enhance intermolecular interactions such as C–H \cdots π , π – π , halogen and hydrogen bonding between the host and the guest molecules.

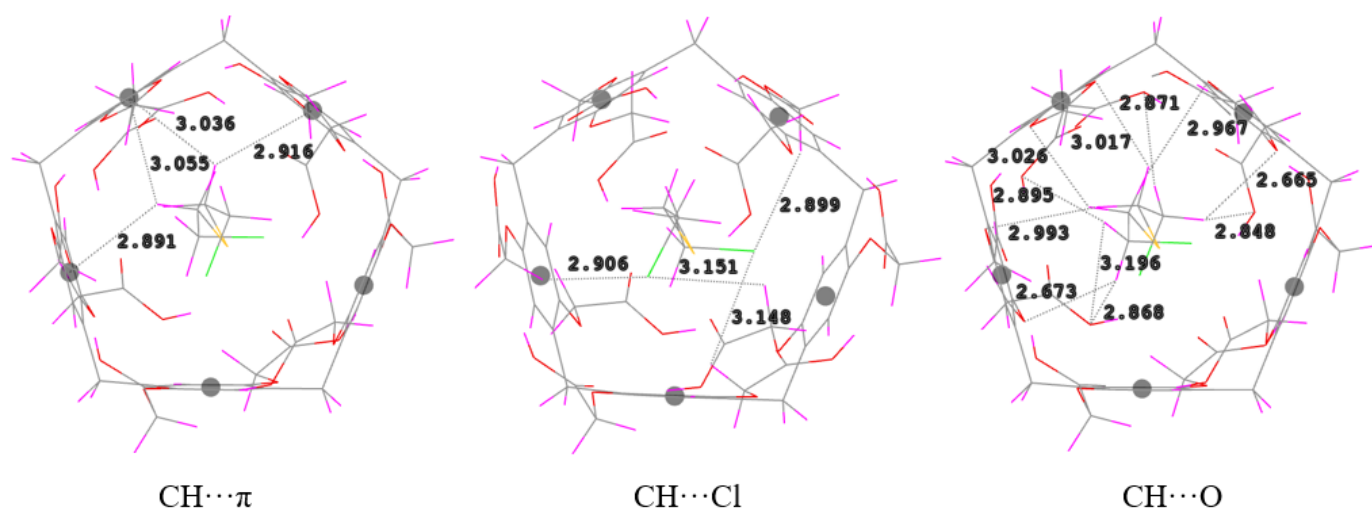


Figure 4. CH $\cdots\pi$, CH \cdots Cl and CH \cdots O hydrogen bonding interactions in the complex SM@DCMP[5].

The host systems selected in this study have more functional groups and could exhibit improved sensing properties towards SM. The electronic quantum parameters such as HOMO and LUMO energies, HOMO–LUMO energy gap ($|\Delta E|_{\text{gap}}$), as well as the percentage of variation of HOMO–LUMO gap were calculated in the gas phase with the r^2 SCAN-3c composite method for the host molecules and their complexes with SM, are reported in Table 5.

Table 5. Calculated HOMO, LUMO, HOMO-LUMO energy gap and the percentage of variation of HOMO–LUMO gap of studied complexes with r^2 SCAN-3c in gas phase.

Host/Complex	Electronic Chemical Parameters			
	E_{HOMO} (eV)	E_{LUMO} (eV)	$ \Delta E _{\text{gap}}$ (eV)	$\Delta E_{\text{g}} \%$
β -CD	−6.14	−0.03	6.11	23.73
SM@ β -CD	−5.98	−1.32	4.66	
CB[6]	−5.82	−0.07	5.75	30.78
SM@CB[6]	−4.21	−0.23	3.98	
P[5]	−4.54	−1.49	3.05	0.00
SM@P[5]	−4.70	−1.65	3.05	
MeP[5]	−4.44	−0.92	3.52	6.82
SM@MeP[5]	−4.40	−1.12	3.28	
DCMP[5]	−5.10	−1.79	3.31	4.83
SM@DCMP[5]	−5.23	−1.76	3.47	
DAP[5]	−4.56	−3.01	1.55	9.03
SM@DAP[5]	−4.56	−2.87	1.69	
CX[5]	−5.44	−1.26	4.18	14.35
SM@CX[5]	−5.14	−1.56	3.58	
P[5]Q	−6.68	−4.73	1.95	51.28
SM@P[5]Q	−5.88	−4.93	0.95	

The results of Table 5 show that after complexation of SM with host molecules, the $|H-L|$ gap of SM@ β -CD, SM@CB[6], SM@MeP[5], SM@CX[5] and SM@P[5]Q complexes decreases, respectively, from 6.11, 5.75, 3.52, 4.18, and 1.95 eV to 4.66, 3.98, 3.28, 3.58 and 0.95 eV, whereas it increases for SM@DCMP[5] and SM@DAP[5] complexes from 3.31 and 1.55 eV to 3.47 and 1.69 eV, respectively. However, the encapsulation of SM in P[5] does not affect the HOMO-LUMO gap energy.

The percentage variation in HOMO–LUMO gap $|\Delta E_{\text{gap}}|$ upon the SM inclusion varies by 51.28, 30.78, 23.73, and 14.35 %, respectively, for SM@P[5]Q, SM@CB[6], SM@ β -CD, and SM@CX[5] complexes, thus showing the potential of these macrocycles as a promising candidate for electronic sensing of SM.

A pictorial representation of frontier molecular orbitals (HOMO and LUMO) of SM@ β -CD, SM@CB[6], SM@CX[5] and SM@P[5]Q using AVOGADRO [98,99] is illustrated in Figure 5.

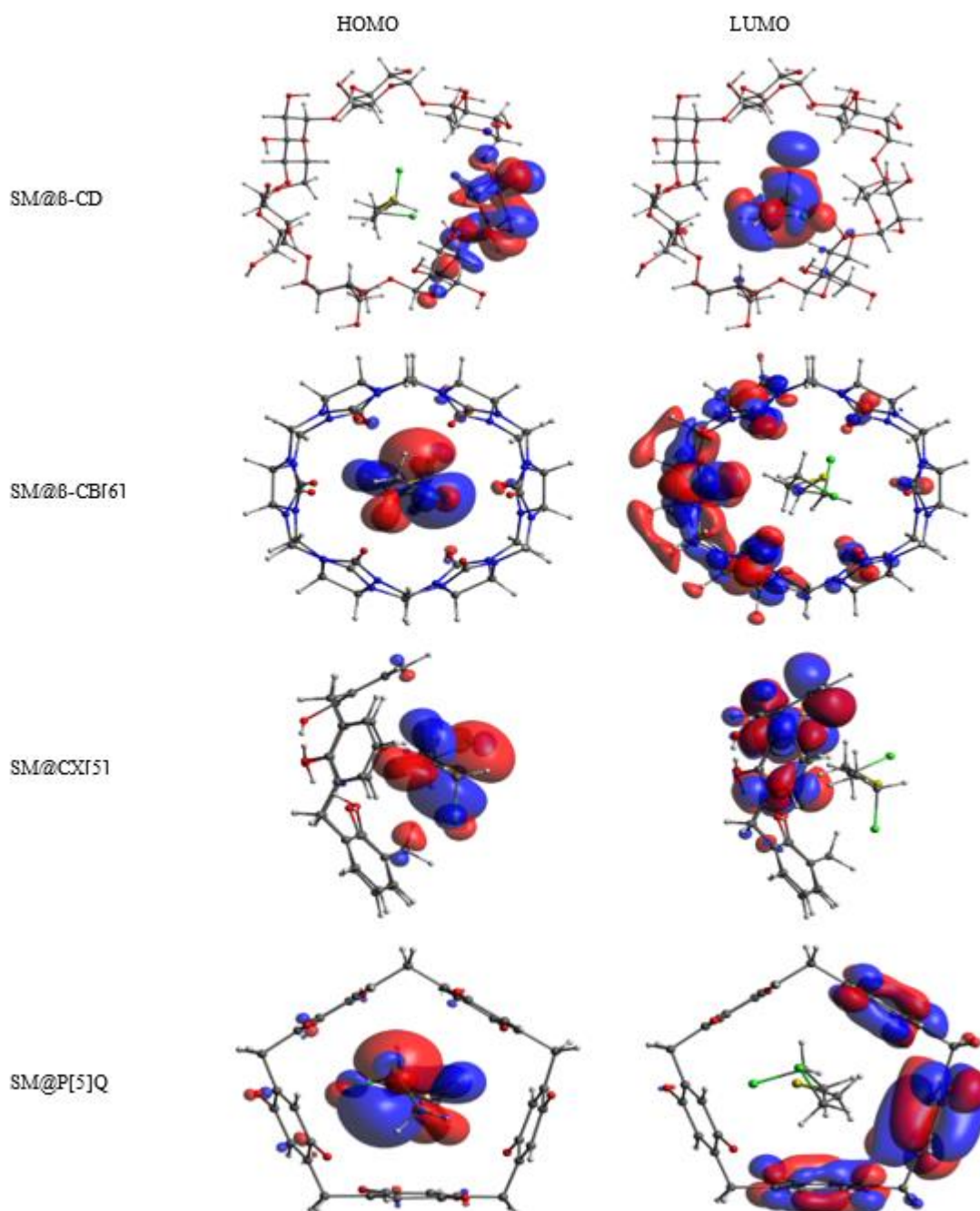


Figure 5. The frontier molecular orbitals (HOMO and LUMO) of SM@ β -CD, SM@CB[6], SM@CX[5], and SM@P[5]Q obtained from r_2 SCAN-3c gas-phase calculations. Atom colors: chlorine (green); oxygen (red); carbon (grey); sulfur (yellow); nitrogen (blue) and hydrogen (white).

The HOMO and LUMO of SM@P[5], SM@DAP[5], SM@MeP[5], and SM@DCMP[5] are presented in Supplementary Figure S2.

The HOMO levels of SM@CB[6], SM@CX[5], and SM@P[5]Q complexes are mainly localized on SM and LUMO levels are localized on the host molecules (CB[6], CX[5], and P[5]Q), whereas the reverse is true for SM@ β -CD complex. It is important to underline that the HOMO energies of SM@ β -CD, SM@CB[6], SM@CX[5], and SM@P[5]Q increase from -6.14 , -5.82 , -5.44 , and -6.68 eV to -5.98 , -4.21 , -5.14 , and -5.88 eV and the LUMO energies decrease from -0.03 , -0.07 , -1.26 , and -4.73 eV to -1.32 , -0.23 , -1.56 , and -4.93 eV, respectively, this destabilization of HOMO energies and stabilization of LUMO energies leads to a significant reduction of the |H-L| gap and, therefore, the increase of the sensitivity and reactivity of β -CD, CB[6], CX[5] and P[5]Q hosts towards SM.

3.2.2. NCI-RDG Analysis of SM@DCMP[5] Complex

The results of NCI-RDG analysis show that in addition to the peaks (Figure 6) appearing between -0.01 and 0.00 a.u. of C-H \cdots H-C, S \cdots π , C-H \cdots Cl, C-H \cdots O, and C-H \cdots π intermolecular interactions, the complex SM@DCMP[5] exhibit mainly C-H \cdots H-C, C-H \cdots O-C, and C-H \cdots O-H intramolecular interactions in the range (-0.03 , -0.02 a.u.). The spikes appearing at ~ -0.03 a.u. in Figure 6 (right) correspond to the intramolecular hydrogen bonds as revealed by the presence of four blue-colored disc-shaped isosurfaces (Figure 6-left) with O \cdots H distances less than 2.0 Å (1.87 , 1.87 , 1.92 , and 1.92 Å). Thus, these intramolecular hydrogen bonds contribute to stabilizing the complex SM@DCMP[5]. It is worth mentioning that the carboxyl end groups are remarkably pointing to the interior of DCMP[5] cavity upon the SM inclusion, allowing, therefore, the formation of a circular intramolecular hydrogen-bond network. Moreover, the SM is totally sequestered in the cavity of DCMP[5].

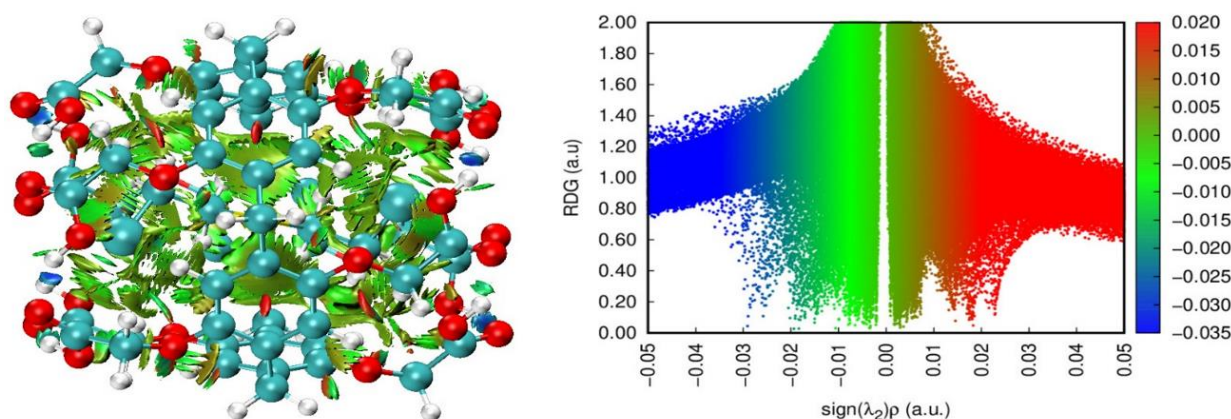


Figure 6. NCI-RDG isosurface (isovalued 0.5 a.u.) (left) and scatter plot (right) of SM@DCMP[5].

4. Conclusions

The present investigation aimed at providing an insight into the in-depth understanding of the interactions governing the structure and host-guest complexation of sulfur mustard and its derivatives with different macrocyclic systems using the newly developed composite method r^2 SCAN-3c. The analysis of the obtained results comes to the following conclusions:

- The r^2 SCAN-3c method can reproduce satisfactorily the crystalline structures of SM@EtP[5], S1@EtP[5], S2@EtP[5], S3@EtP[5], S4@EtP[5], and S5@EtP[5] complexes.
- The complexation energies calculated using r^2 SCAN-3c correlate with the experimental association constants.
- The major forces that contribute to the stability of the formed complexes involve C-H \cdots H-C, C-H \cdots O intramolecular interactions and C-H \cdots H-C, S \cdots π , C-H \cdots Cl, C-H \cdots S, C-H \cdots O and C-H \cdots π intermolecular interactions as revealed by NCI-RDG and IGM analysis.

- The macrocycles CB[6], β -CD, CX[5] and particularly P[5]Q show great potential as sensors for sulfur mustard.
- Among the studied complexes, SM@DCMP[5] was the most stable with the highest complexation energy of -155.26 kJ/mol, its high stability is due to the occurrence of additional intramolecular hydrogen bonds in DCMP[5].

Supplementary Materials: The following supporting information can be downloaded at: <https://www.mdpi.com/article/10.3390/nano12152517/s1>, Figure S1: IGMH isosurfaces (isovalue 0.007 a.u.) (upper figures) and scatter plots (lower figures) of SM@EtP[5], S1@EtP[5], S2@EtP[5], S3@EtP[5], S4@EtP[5] and S5@EtP[5]; Figure S2: The frontier molecular orbitals (HOMO and LUMO) of SM@P[5], SM@DAP[5], SM@MeP[5] and SM@DCMP[5] obtained from r^2 SCAN-3c gas phase calculations.

Author Contributions: Conceptualization, Y.B. and N.A.; methodology, S.R., Y.B. and R.B.S.; software, S.R., R.B.S. and F.A.M.; validation, Y.B., N.A., F.A.M.A., H.A. and M.G.G.; formal analysis, F.A.M., R.B.S. and S.R.; investigation, Y.B., N.A., S.R. and F.A.M.; resources, F.A.M.A., H.A. and M.G.G.; data curation, F.A.M. and S.R.; writing—original draft preparation, F.A.M., S.R. and N.A.; writing—review and editing, Y.B., F.A.M.A., H.A. and M.G.G.; visualization, F.A.M. and R.B.S.; supervision, Y.B. and N.A.; project administration, Y.B.; funding acquisition, F.A.M.A., H.A. and M.G.G. All authors have read and agreed to the published version of the manuscript.

Funding: This research received no external funding.

Institutional Review Board Statement: Not applicable.

Informed Consent Statement: Not applicable.

Data Availability Statement: The data presented in this study are available on request from the corresponding author.

Conflicts of Interest: The authors declare no conflict of interest.

References

1. Facts About Sulfur Mustard. Available online: <https://emergency.cdc.gov/agent/sulfurmustard/basics/facts.asp> (accessed on 29 December 2021).
2. Wormser, U. Toxicology of mustard gas. *Trends Pharmacol. Sci.* **1991**, *12*, 164–167. [[CrossRef](#)]
3. Smith, S.L. *Toxic Exposures: Sulfur Mustard and the Health Consequences of World War II in the United States*; Rutgers University Press: New Brunswick, NJ, USA, 2017.
4. Duchovic, R.J.; Vilensky, J.A. Mustard sulfur: Its pre-World War I history. *J. Chem. Educ.* **2007**, *84*, 944. [[CrossRef](#)]
5. Norman, J.E., Jr. Lung cancer mortality in World War I veterans with mustard-gas injury: 1919–1965. *J. Natl. Cancer Inst.* **1975**, *54*, 311–317. [[CrossRef](#)]
6. Razavi, S.M.; Ghanei, M.; Salamati, P.; Safiabadi, M. Long-term effects of mustard gas on respiratory system of Iranian veterans after Iraq-Iran war: A review. *Chin. J. Traumatol.* **2013**, *16*, 163–168. [[PubMed](#)]
7. Liu, Y.; Howarth, A.J.; Vermeulen, N.A.; Moon, S.-Y.; Hupp, J.T.; Farha, O.K. Catalytic degradation of chemical warfare agents and their simulants by metal-organic frameworks. *Coord. Chem. Rev.* **2017**, *346*, 101–111. [[CrossRef](#)]
8. Wang, Q.-Q.; Begum, R.A.; Day, V.W.; Bowman-James, K. Chemical mustard containment using simple palladium pincer complexes: The influence of molecular walls. *J. Am. Chem. Soc.* **2013**, *135*, 17193–17199. [[CrossRef](#)]
9. Islamoglu, T.; Chen, Z.; Wasson, M.C.; Buru, C.T.; Kirlikovali, K.O.; Afrin, U.; Mian, M.R.; Farha, O.K. Metal-Organic Frameworks against Toxic Chemicals. *Chem. Rev.* **2020**, *120*, 8130–8160. [[CrossRef](#)]
10. Plass, W. Supramolecular interactions of vanadate species: Vanadium (V) complexes with N-salicylidenehydrazides as versatile models. *Coord. Chem. Rev.* **2003**, *237*, 205–212. [[CrossRef](#)]
11. Zhao, D.; Yu, S.; Jiang, W.-J.; Cai, Z.-H.; Li, D.-L.; Liu, Y.-L.; Chen, Z.-Z. Recent Progress in Metal-Organic Framework Based Fluorescent Sensors for Hazardous Materials Detection. *Molecules* **2022**, *27*, 2226. [[CrossRef](#)] [[PubMed](#)]
12. Litim, A.; Belhocine, Y.; Benlecheb, T.; Ghoniem, M.G.; Kabouche, Z.; Ali, F.A.M.; Abdulkhair, B.Y.; Seydou, M.; Rahali, S. DFT-D4 Insight into the Inclusion of Amphetamine and Methamphetamine in Cucurbit [7] uril: Energetic, Structural and Biosensing Properties. *Molecules* **2021**, *26*, 7479. [[CrossRef](#)]
13. Novikov, A.S. Non-Covalent Interactions in Organic, Organometallic, and Inorganic Supramolecular Systems Relevant for Medicine, Materials Science, and Catalysis. *Crystals* **2022**, *12*, 246. [[CrossRef](#)]
14. Bouhadiba, A.; Rahali, S.; Belhocine, Y.; Allal, H.; Nouar, L.; Rahim, M. Structural and energetic investigation on the host/guest inclusion process of benzyl isothiocyanate into β -cyclodextrin using dispersion-corrected DFT calculations. *Carbohydr. Res.* **2020**, *491*, 107980. [[CrossRef](#)] [[PubMed](#)]

15. Maharramov, A.M.; Mahmudov, K.T.; Kopylovich, M.N.; Pombeiro, A.J.L. (Eds.) *Noncovalent Interactions in the Synthesis and Design of New Compounds*; John Wiley & Sons: Hoboken, NJ, USA, 2016.
16. Várnai, B.; Zsila, F.; Szakács, Z.; Garádi, Z.; Malanga, M.; Béni, S. Sulfobutylation of Beta-Cyclodextrin Enhances the Complex Formation with Mitragynine: An NMR and Chiroptical Study. *Int. J. Mol. Sci.* **2022**, *23*, 3844. [[CrossRef](#)]
17. Cid-Samamed, A.; Rakmai, J.; Mejuto, J.C.; Simal-Gandara, J.; Astray, G. Cyclodextrins inclusion complex: Preparation methods, analytical techniques and food industry applications. *Food Chem.* **2022**, *384*, 132467. [[CrossRef](#)]
18. Assaba, I.M.; Rahali, S.; Belhocine, Y.; Allal, H. Inclusion complexation of chloroquine with α and β -cyclodextrin: Theoretical insights from the new B97-3c composite method. *J. Mol. Struct.* **2021**, *1227*, 129696. [[CrossRef](#)]
19. Wdowiak, K.; Rosiak, N.; Tykarska, E.; Żarowski, M.; Płazińska, A.; Płaziński, W.; Cielecka-Piontek, J. Amorphous Inclusion Complexes: Molecular Interactions of Hesperidin and Hesperetin with HP-B-CD and Their Biological Effects. *Int. J. Mol. Sci.* **2022**, *23*, 4000. [[CrossRef](#)]
20. Baudin, C.; Pean, C.; Perly, B.; Gosselin, P. Inclusion of organic pollutants in cyclodextrin and derivatives. *Int. J. Environ. Anal. Chem.* **2000**, *77*, 233–242. [[CrossRef](#)]
21. Del Valle, E.M.M. Cyclodextrins and their uses: A review. *Process Biochem.* **2004**, *39*, 1033–1046. [[CrossRef](#)]
22. Crini, G. Review: A history of cyclodextrins. *Chem. Rev.* **2014**, *114*, 10940–10975. [[CrossRef](#)]
23. Masson, E.; Ling, X.X.; Joseph, R.; Kyeremeh-Mensah, L.; Lu, X.Y. Cucurbituril chemistry: A tale of supramolecular success. *RSC Adv.* **2012**, *2*, 1213–1247. [[CrossRef](#)]
24. Assaf, K.L.; Nau, W.M. Cucurbiturils: From synthesis to high-affinity binding and catalysis. *Chem. Soc. Rev.* **2015**, *44*, 394–418. [[CrossRef](#)]
25. Barrow, S.J.; Kaser, S.; Rowland, M.J.; del Barrio, J.; Scherman, O.A. Cucurbituril-based molecular recognition. *Chem. Rev.* **2015**, *115*, 12320–12406. [[CrossRef](#)]
26. Español, E.S.; Villamil, M.M. Calixarenes: Generalities and Their Role in Improving the Solubility, Biocompatibility, Stability, Bioavailability, Detection, and Transport of Biomolecules. *Biomolecules* **2019**, *9*, 90. [[CrossRef](#)] [[PubMed](#)]
27. Kumar, R.; Sharma, A.; Singh, H.; Suating, P.; Kim, H.S.; Sunwoo, K.; Shim, I.; Gibb, B.C.; Kim, J.S. Revisiting Fluorescent Calixarenes: From Molecular Sensors to Smart Materials. *Chem. Rev.* **2019**, *119*, 9657–9721. [[CrossRef](#)] [[PubMed](#)]
28. Kumar, S.; Chawla, S.; Zou, M.C. Calixarenes based materials for gas sensing applications: A review. *J. Incl. Phenom. Macrocycl. Chem.* **2017**, *88*, 129–158. [[CrossRef](#)]
29. Koifman, O.I.; Ageeva, T.A.; Beletskaya, I.P.; Averin, A.D.; Yakushev, A.A.; Tomilova, L.G.; Dubinina, T.V.; Tsvadze, A.Y.; Gorbunova, Y.G.; Stuzhin, P.A.; et al. Macroheterocyclic Compounds—A Key Building Block in New Functional Materials and Molecular Devices. *Macroheterocycles* **2020**, *13*, 311–467. [[CrossRef](#)]
30. Xue, M.; Yang, Y.; Chi, X.; Zhang, Z.; Huang, F. Pillararenes, A New Class of Macrocycles for Supramolecular Chemistry. *Acc. Chem. Res.* **2012**, *45*, 1294–1308. [[CrossRef](#)]
31. Guo, F.; Sun, Y.; Xi, B.; Diao, G. Recent progress in the research on the host-guest chemistry of pillar[n]arenes. *Supramol. Chem.* **2018**, *30*, 81–92. [[CrossRef](#)]
32. Ogoshi, T.; Kanai, S.; Fujinami, S.; Yamagishi, T.A.; Nakamoto, Y. *para*-Bridged symmetrical Pillar[5]arenes: Their Lewis acid catalyzed synthesis and host-guest property. *J. Am. Chem. Soc.* **2008**, *130*, 5022–5023. [[CrossRef](#)]
33. Gu, R.; Lehn, J.-M. Constitutional Dynamic Selection at Low Reynolds Number in a Triple Dynamic System: Covalent Dynamic Adaptation Driven by Double Supramolecular Self-Assembly. *J. Am. Chem. Soc.* **2021**, *143*, 14136–14146. [[CrossRef](#)]
34. Wang, S.; Li, X.; Zhang, X.; Huang, P.; Fang, P.; Wang, J.; Yang, S.; Wu, K.; Du, P. A supramolecular polymeric heterojunction composed of an all-carbon conjugated polymer and fullerenes. *Chem. Sci.* **2021**, *12*, 10506–10513. [[CrossRef](#)]
35. Lou, X.Y.; Song, N.; Yang, Y.W. A stimuli-responsive pillararene-based hybrid material with enhanced tunable multicolor luminescence and ion-sensing ability. *Natl. Sci. Rev.* **2021**, *8*, nwaa281. [[CrossRef](#)] [[PubMed](#)]
36. Ruan, Y.; Li, Q.-H.; Shu, L.; Wan, J.-H. A Shape-Persistent Arylene Ethynylene Macrocyclic with a Multiple Acetamide Modified Cavity: Synthesis and Gelation. *Soft Matter* **2021**, *17*, 3242–3249. [[CrossRef](#)] [[PubMed](#)]
37. Xing, R.; Liu, K.; Jiao, T.; Zhang, N.; Ma, K.; Zhang, R.; Zou, Q.; Ma, G.; Yan, X. An injectable self-assembling collagen-gold hybrid hydrogel for combinatorial antitumor photothermal/photodynamic therapy. *Adv. Mater.* **2016**, *28*, 3669–3676. [[CrossRef](#)]
38. Song, J.; Yuan, C.; Jiao, T.; Xing, R.; Yang, M.; Adams, D.J.; Yan, X. Multifunctional antimicrobial biometallohydrogels based on amino Acid coordinated self-assembly. *Small* **2020**, *16*, 1907309. [[CrossRef](#)] [[PubMed](#)]
39. Li, B.; Li, S.; Wang, B.; Meng, Z.; Wang, Y.; Meng, Q.; Li, C. Capture of sulfur mustard by pillar[5]arene: From host-guest complexation to efficient adsorption using nonporous adaptive crystals. *iScience* **2020**, *23*, 101443. [[CrossRef](#)]
40. Zhou, S.; Li, W.; Zhao, Q.; Dong, H.; Wang, Y.; Lu, F.; Zhao, J.; Liu, S.; Chen, H.; Wang, L.; et al. Detoxification of the Toxic Sulfur Mustard Simulant by a Supramolecular Antidote in Vitro and in Vivo. *ACS Appl. Mater. Interfaces* **2021**, *13*, 58291–58300. [[CrossRef](#)] [[PubMed](#)]
41. De Souza, L.A.; Nogueira, C.A.S.; Lopes, J.F.; Dos Santos, H.F.; De Almeida, W.B. DFT study of cisplatin@carbon nanohorns complexes. *J. Inorg. Biochem.* **2013**, *129*, 71–83. [[CrossRef](#)]
42. Belhocine, Y.; Bouhadiba, A.; Rahim, M.; Nouar, L.; Djilani, I.; Khatmi, D.I. Inclusion Complex Formation of β -Cyclodextrin with the Nonsteroidal Anti-inflammatory Drug Flufenamic Acid: Computational Study. *Macroheterocycles* **2018**, *11*, 203–209. [[CrossRef](#)]

43. Aree, T.; Jongrungruangchok, S. Structure–antioxidant activity relationship of β -cyclodextrin inclusion complexes with olive tyrosol, hydroxytyrosol and oleuropein: Deep insights from X-ray analysis, DFT calculation and DPPH assay. *Carbohydr. Polym.* **2018**, *199*, 661–669. [[CrossRef](#)]
44. Buta, M.C.; Toader, A.M.; Frecus, B.; Oprea, C.I.; Cimpoesu, F.; Ionita, G. Molecular and Supramolecular Interactions in Systems with Nitroxide-Based Radicals. *Int. J. Mol. Sci.* **2019**, *20*, 4733. [[CrossRef](#)] [[PubMed](#)]
45. Xie, J.; Shen, C.; Shi, H.; Luo, S.; He, M.; Chen, M. Theoretical prediction of structures and inclusion properties of heteroatom-bridged pillar[n]arenes. *Struct. Chem.* **2020**, *31*, 329–337. [[CrossRef](#)]
46. Nikolova, V.; Velinova, A.; Dobrev, S.; Kircheva, N.; Angelova, S.; Dudev, T. Host–Guest Complexation of Cucurbit[7]Urill and Cucurbit[8]Urill with the Antineoplastic and Multiple Sclerosis Agent Mitoxantrone (Novantrone). *J. Phys. Chem. A* **2021**, *125*, 536–542. [[CrossRef](#)]
47. Venkataramanan, N.S.; Suvitha, A.; Mizuseki, H.; Kawazoe, Y. Computational study on the interactions of mustard gas with cucurbituril macrocycles. *Int. J. Quantum Chem.* **2015**, *115*, 1515–1525. [[CrossRef](#)]
48. Venkataramanan, N.S.; Ambigapathy, S. Encapsulation of sulfur, oxygen, and nitrogen mustards by cucurbiturils: A DFT study. *J. Incl. Phenom. Macrocycl. Chem.* **2015**, *83*, 387–400. [[CrossRef](#)]
49. Grimme, S.; Hansen, A.; Ehlert, S.; Mewes, J.M. r²SCAN-3c: A “Swiss army knife” composite electronic-structure method. *J. Chem. Phys.* **2021**, *154*, 064103. [[CrossRef](#)]
50. Furness, J.W.; Kaplan, A.D.; Ning, J.; Perdew, J.P.; Sun, J. Accurate and Numerically Efficient r²SCAN Meta-Generalized Gradient Approximation. *J. Phys. Chem. Lett.* **2020**, *11*, 8208–8215, Erratum in *J. Phys. Chem. Lett.* **2020**, *11*, 9248. [[CrossRef](#)]
51. Santra, G.; Martin, J.M.L. Pure and Hybrid SCAN, rSCAN, and r²SCAN: Which One Is Preferred in KS- and HF-DFT Calculations, and How Does D4 Dispersion Correction Affect This Ranking? *Molecules* **2022**, *27*, 141. [[CrossRef](#)]
52. Kingsbury, R.; Gupta, A.; Bartel, C.; Munro, J.; Dwaraknath, S.; Horton, M.; Persson, K. Performance comparison of r²SCAN and SCAN metaGGA density functionals for solid materials via an automated, high-throughput computational workflow. *Phys. Rev. Mater.* **2022**, *6*, 013801. [[CrossRef](#)]
53. Ehlert, S.; Grimme, S.; Hansen, A. Conformational Energy Benchmark for Longer n-Alkane Chains. *J. Phys. Chem. A* **2022**, *126*, 3521–3535. [[CrossRef](#)]
54. Furness, J.W.; Kaplan, A.D.; Ning, J.; Perdew, J.P.; Sun, J. Construction of meta-GGA functionals through restoration of exact constraint adherence to regularized SCAN functionals. *J. Chem. Phys.* **2021**, *156*, 034109. [[CrossRef](#)] [[PubMed](#)]
55. Ehlert, S.; Huniar, U.; Ning, J.; Furness, J.W.; Sun, J.; Kaplan, A.D.; Perdew, J.P.; Brandenburg, J.G. r²SCAN-D4: Dispersion corrected meta-generalized gradient approximation for general chemical applications. *J. Chem. Phys.* **2021**, *154*, 061101. [[CrossRef](#)] [[PubMed](#)]
56. Grimm, L.M.; Spicher, S.; Tkachenko, B.; Schreiner, P.R.; Grimme, S.; Biedermann, F. The Role of Packing, Dispersion, Electrostatics, and Solvation in High-Affinity Complexes of Cucurbit[n]urils with Uncharged Polar Guests. *Chem. A Eur. J.* **2022**, *28*, e202200529. [[CrossRef](#)] [[PubMed](#)]
57. Bursch, M.; Mewes, J.-M.; Hansen, A.; Grimme, S. *Best Practice DFT Protocols for Basic Molecular Computational Chemistry*; Cambridge Open Engage: Cambridge, UK, 2022.
58. Weigend, F.; Ahlrichs, R. Balanced basis sets of split valence, triple zeta valence and quadruple zeta valence quality for H to Rn: Design and assessment of accuracy. *Phys. Chem. Phys. Chem.* **2005**, *7*, 3297–3305. [[CrossRef](#)] [[PubMed](#)]
59. Kruse, H.; Grimme, S. A geometrical correction for the inter- and intra-molecular basis set superposition error in Hartree-Fock and density functional theory calculations for large systems. *J. Chem. Phys.* **2012**, *136*, 154101. [[CrossRef](#)]
60. Caldeweyher, E.; Bannwarth, C.; Grimme, S. Extension of the D3 dispersion coefficient model. *J. Chem. Phys.* **2017**, *147*, 034112. [[CrossRef](#)]
61. Caldeweyher, E.; Ehlert, S.; Hansen, A.; Neugebauer, H.; Spicher, S.; Bannwarth, C.; Grimme, S. A generally applicable atomic-charge dependent London dispersion correction. *J. Chem. Phys.* **2019**, *150*, 154122. [[CrossRef](#)]
62. Caldeweyher, E.; Mewes, J.-M.; Ehlert, S.; Grimme, S. Extension and evaluation of the D4 London-dispersion model for periodic systems. *Phys. Chem. Chem. Phys.* **2020**, *22*, 8499–8512. [[CrossRef](#)]
63. Neese, F. The ORCA program system. *Wiley Interdiscip. Rev. Comput. Mol. Sci.* **2012**, *2*, 73–78. [[CrossRef](#)]
64. Neese, F. Software update: The ORCA program system, version 4.0. *Wiley Interdiscip. Rev. Comput. Mol. Sci.* **2017**, *8*, e1327. [[CrossRef](#)]
65. Neese, F.; Wennmohs, F.; Becker, U.; Riplinger, C. The ORCA quantum chemistry program package. *J. Chem. Phys.* **2020**, *152*, 224108. [[CrossRef](#)] [[PubMed](#)]
66. Cossi, M.; Rega, N.; Scalmani, G.; Barone, V. Energies, structures, and electronic properties of molecules in solution with the C-PCM solvation model. *J. Comput. Chem.* **2003**, *24*, 669–681. [[CrossRef](#)] [[PubMed](#)]
67. Barone, V.; Cossi, M. Quantum calculation of molecular energies and energy gradients in solution by a conductor solvent model. *J. Phys. Chem. A* **1998**, *102*, 1995–2001. [[CrossRef](#)]
68. Li, B.; Li, S.; Wang, B.; Meng, Z.; Wang, Y.; Meng, Q.; Li, C. *CCDC 1831237: Experimental Crystal Structure Determination*; CCDC: Cambridge, UK, 2020. [[CrossRef](#)]
69. Li, B.; Li, S.; Wang, B.; Meng, Z.; Wang, Y.; Meng, Q.; Li, C. *CCDC 1884850: Experimental Crystal Structure Determination*; CCDC: Cambridge, UK, 2020. [[CrossRef](#)]

70. Li, B.; Li, S.; Wang, B.; Meng, Z.; Wang, Y.; Meng, Q.; Li, C. CCDC 1831239: *Experimental Crystal Structure Determination*; CCDC: Cambridge, UK, 2020. [[CrossRef](#)]
71. Li, B.; Li, S.; Wang, B.; Meng, Z.; Wang, Y.; Meng, Q.; Li, C. CCDC 1884851: *Experimental Crystal Structure Determination*; CCDC: Cambridge, UK, 2020. [[CrossRef](#)]
72. Li, B.; Li, S.; Wang, B.; Meng, Z.; Wang, Y.; Meng, Q.; Li, C. CCDC 1831240: *Experimental Crystal Structure Determination*; CCDC: Cambridge, UK, 2020. [[CrossRef](#)]
73. Li, B.; Li, S.; Wang, B.; Meng, Z.; Wang, Y.; Meng, Q.; Li, C. CCDC 1884852: *Experimental Crystal Structure Determination*; CCDC: Cambridge, UK, 2020. [[CrossRef](#)]
74. MacRae, C.F.; Sovago, I.; Cottrell, S.J.; Galek, P.T.A.; McCabe, P.; Pidcock, E.; Platings, M.; Shields, G.P.; Stevens, J.S.; Towler, M.; et al. Mercury 4.0: From visualization to analysis, design and prediction. *J. Appl. Cryst.* **2020**, *53*, 226–235. [[CrossRef](#)] [[PubMed](#)]
75. Piya, A.A.; Shamim, S.U.D.; Uddin, M.N.; Munny, K.N.; Alam, A.; Hossain, M.K.; Ahmed, F. Adsorption behavior of cisplatin anticancer drug on the pristine, Al- and Ga-doped BN nanosheets: A comparative DFT study. *Comput. Theor. Chem.* **2021**, *1200*, 113241. [[CrossRef](#)]
76. Rezaei, A.; Ghiasi, R.; Marjani, A. Strong chemisorption of E₂H₂ and E₂H₄ (E = C, Si) on B₁₂N₁₂ nano-cage. *J. Nanostruct. Chem.* **2020**, *10*, 179–191. [[CrossRef](#)]
77. Ding, S.; Gu, W. Evaluate the potential utilization of B₂₄N₂₄ fullerene in the recognition of COS, H₂S, SO₂, and CS₂ gases (environmental pollution). *J. Mol. Liq.* **2022**, *345*, 117041. [[CrossRef](#)]
78. Fifere, A.; Marangoci, N.; Maier, S.S.; Coroaba, A.; Maftei, D.; Pinteala, M. Theoretical study on β -cyclodextrin inclusion complexes with propiconazole and protonated propiconazole. *Beilstein J. Org. Chem.* **2012**, *8*, 2191–2201. [[CrossRef](#)]
79. Biedermann, F.; Schneider, H.-J. Experimental binding energies in supramolecular complexes. *Chem. Rev.* **2016**, *116*, 5216–5300. [[CrossRef](#)]
80. Saleh, G.; Gatti, C.; Lo Presti, L. Non-covalent interaction via the reduced density gradient: Independent atom model vs experimental multipolar electron densities. *Comput. Theor. Chem.* **2012**, *998*, 148–163. [[CrossRef](#)]
81. Lu, T.; Chen, Q. Independent gradient model based on Hirshfeld partition: A new method for visual study of interactions in chemical systems. *J. Comput. Chem.* **2022**, *43*, 539–555. [[CrossRef](#)] [[PubMed](#)]
82. Humphrey, W.; Dalke, A.; Schulten, K. VMD—Visual Molecular Dynamics. *J. Mol. Graph.* **1996**, *14*, 33–38. [[CrossRef](#)]
83. Lu, T.; Chen, F. Multiwfn: A multifunctional wavefunction analyzer. *J. Comput. Chem.* **2012**, *33*, 580–592. [[CrossRef](#)] [[PubMed](#)]
84. Tsuzuki, S. CH/ π Interactions. Annual Reports Section “C”. *Phys. Chem.* **2012**, *108*, 69–95.
85. Ogoshi, T.; Aoki, T.; Kitajima, K.; Fujinami, S.; Yamagishi, T.-A.; Nakamoto, Y. Facile, rapid, and high-yield synthesis of pillar[5]arene from commercially available reagents and its X-ray crystal structure. *J. Org. Chem.* **2011**, *76*, 328–331. [[CrossRef](#)] [[PubMed](#)]
86. Li, C.; Shu, X.; Li, J.; Chen, S.; Han, K.; Xu, M.; Jia, X. Complexation of 1,4-Bis(pyridinium)butanes by negatively charged carboxylatopillar[5]arene. *J. Org. Chem.* **2011**, *76*, 8458–8465. [[CrossRef](#)]
87. Shurpik, D.N.; Yakimova, L.S.; Makhmutova, L.I.; Makhmutova, A.R.; Rizvanov, I.K.; Plemenkov, V.V.; Stoikov, I.I. Pillar[5]arenes with morpholide and pyrrolidide substituents: Synthesis and complex formation with alkali metal ions. *Macroheterocycles* **2014**, *7*, 351–357. [[CrossRef](#)]
88. Yakimova, L.S.; Shurpik, D.N.; Makhmutova, A.R.; Stoikov, I.I. pillar[5]arenes bearing amide and carboxylic groups as synthetic receptors for alkali metal ions. *Macroheterocycles* **2017**, *10*, 226–232. [[CrossRef](#)]
89. Shivakumar, K.I.; Yan, Y.; Hughes, C.E.; Apperley, D.C.; Harris, K.D.M.; Sanjayan, G.J. Exploiting powder X-ray diffraction to establish the solvent-assisted solid-state supramolecular assembly of pillar[5]quinone. *Cryst. Growth Des.* **2015**, *15*, 1583–1587. [[CrossRef](#)]
90. Strutt, N.L.; Zhang, H.; Schneebeli, S.T.; Stoddart, J.F. Amino-functionalized pillar[5]arene. *Chemistry* **2014**, *20*, 10996–11004. [[CrossRef](#)]
91. Chen, K.; Kang, Y.S.; Zhao, Y.; Yang, J.M.; Lu, Y.; Sun, W.Y. Cucurbit[6]uril-based supramolecular assemblies: Possible application in radioactive cesium cation capture. *J. Am. Chem. Soc.* **2014**, *136*, 16744–16747. [[CrossRef](#)] [[PubMed](#)]
92. Dalgarno, S.J.; Tian, J.; Warren, J.E.; Clark, T.E.; Makha, M.; Raston, C.L.; Atwood, J.L. Calix[5]arene: A versatile sublimate that displays gas sorption properties. *Chem. Commun.* **2007**, *46*, 4848–4850. [[CrossRef](#)] [[PubMed](#)]
93. Dalgarno, S.J.; Tian, J.; Warren, J.E.; Clark, T.E.; Makha, M.; Raston, C.L.; Atwood, J.L. CCDC 637165: *Experimental Crystal Structure Determination*; CCDC: Cambridge, UK, 2008. [[CrossRef](#)]
94. Aree, T.; Chaichit, N. Crystal structure of β -cyclodextrin–benzoic acid inclusion complex. *Carbohydr. Res.* **2003**, *338*, 439–446. [[CrossRef](#)]
95. Aree, T.; Chaichit, N. CCDC 191347: *Experimental Crystal Structure Determination*; CCDC: Cambridge, UK, 2003. [[CrossRef](#)]
96. Liu, L.; Guo, Q.-X. Use of quantum chemical methods to study cyclodextrin chemistry. *J. Incl. Phenom. Macrocycl. Chem.* **2004**, *50*, 95–103. [[CrossRef](#)]
97. Dennington, R.; Keith, T.; Millam, J. *GaussView*; Version 5; Semichem Inc.: Shawnee Mission, KS, USA, 2009.

-
98. Hanwell, M.D.; Curtis, D.E.; Lonie, D.C.; Vandermeersch, T.; Zurek, E.; Hutchison, G.R. Avogadro: An advanced semantic chemical editor, visualization, and analysis platform. *J. Cheminformatics* **2012**, *4*, 17. [[CrossRef](#)] [[PubMed](#)]
 99. Avogadro: An Open-Source Molecular Builder and Visualization Tool, Version 1.2.0. Available online: <http://avogadro.cc/> (accessed on 24 May 2022).